



# Direct measurement of the Zak phase in topological Bloch bands

## Citation

Atala, Marcos, Monika Aidelsburger, Julio T. Barreiro, Dmitry Abanin, Takuya Kitagawa, Eugene Demler, and Immanuel Bloch. 2013. "Direct Measurement of the Zak Phase in Topological Bloch Bands." *Nat Phys* 9 (12) (November 3): 795–800.

## Published Version

doi:10.1038/nphys2790

## Permanent link

<http://nrs.harvard.edu/urn-3:HUL.InstRepos:12150777>

## Terms of Use

This article was downloaded from Harvard University's DASH repository, and is made available under the terms and conditions applicable to Other Posted Material, as set forth at <http://nrs.harvard.edu/urn-3:HUL.InstRepos:dash.current.terms-of-use#LAA>

## Share Your Story

The Harvard community has made this article openly available.  
Please share how this access benefits you. [Submit a story](#).

[Accessibility](#)

# Measurement of the Zak phase in Topological Bloch Bands

Marcos Atala,<sup>1,†</sup> Monika Aidelsburger,<sup>1,†</sup> Julio T. Barreiro,<sup>1,2</sup>  
Dmitry Abanin,<sup>3</sup> Takuya Kitagawa,<sup>3</sup> Eugene Demler,<sup>3</sup> Immanuel Bloch<sup>1,2,\*</sup>

<sup>1</sup>Fakultät für Physik, Ludwig-Maximilians-Universität, Schellingstr. 4, 80799 Munich, Germany

<sup>2</sup>Max-Planck Institute of Quantum Optics, Hans-Kopfermann Str. 1, 85748 Garching, Germany

<sup>3</sup>Department of Physics, Harvard University, 17 Oxford Str., Cambridge, MA 02138, USA

\*To whom correspondence should be addressed; E-mail: immanuel.bloch@mpq.mpg.de

<sup>†</sup>These two authors contributed equally to this work.

Monday 23<sup>rd</sup> September, 2013 19:49

**Geometric phases that characterize topological properties of Bloch bands play a fundamental role in the band theory of solids. Here we report on the measurement of the geometric phase acquired by cold atoms moving in one-dimensional optical lattices. Using a combination of Bloch oscillations and Ramsey interferometry, we extract the Zak phase – the Berry phase acquired during an adiabatic motion of a particle across the Brillouin zone – which can be viewed as an invariant characterizing the topological properties of the band. For a dimerized lattice, which models polyacetylene, we measure a difference of the Zak phase  $\delta\varphi_{\text{Zak}} = 0.97(2)\pi$  for the two possible polyacetylene phases with different dimerization. The two dimerized phases therefore belong to different topological classes, such that for a filled band, domain walls have fractional quantum numbers. Our work establishes a new general approach for probing the topological structure of Bloch bands in optical lattices.**

The non-trivial topological structure of Bloch bands in solids gives rise to fundamental physical phenomena, including fermion number fractionalization (1–4), the integer quantum Hall effect (5, 6), as

well as topologically protected surface states in topological insulators (7, 8). The topological character of a Bloch band is defined by certain invariants, which can be expressed in terms of the Berry's phase (9) acquired by a particle during adiabatic motion through the band (6, 8). The most well-known example is the two-dimensional topological invariant, the first Chern number, which is related to the Berry's phase for a contour enclosing the Brillouin zone and determines the quantized value of the Hall conductivity of a filled two-dimensional band (5, 6). For one-dimensional systems, topological invariants of Bloch bands have been discussed theoretically (6, 8, 10–12), however never been measured in any experiment.

Here we present direct measurements of Berry's phase and topological invariants of one-dimensional periodic potentials using systems of ultra-cold atoms in optical lattices. Topological properties of one dimensional solids are characterized by the so-called Zak phase – the Berry's phase picked up by a particle moving across the Brillouin zone (12). For a given Bloch wave  $\psi_k(x)$  with quasimomentum  $k$ , the Zak phase can be conveniently expressed through the cell-periodic Bloch function  $u_k(x) = e^{-ikx}\psi_k(x)$ :

$$\varphi_{\text{Zak}} = i \int_{-G/2}^{G/2} \langle u_k | \partial_k | u_k \rangle dk, \quad (1)$$

where  $G = 2\pi/d$  is the reciprocal lattice vector and  $d$  is the lattice period (12). Non-trivial Zak phases underlie the existence of protected edge states (13, 14), fermion number fractionalization (1–3), and irrationally charged domain walls (15, 16) between topologically distinct one-dimensional solids. These phenomena, initially discussed in the context of quantum field theory (1, 2, 15), later on found condensed matter realizations in polyacetylene (3), described by the celebrated Su-Schrieffer-Heeger (SSH) model, and linearly conjugated diatomic polymers (16).

In our experiment, the key idea is to combine coherent Bloch oscillations with Ramsey interferometry to determine the geometrical Zak phase and reveal the underlying topological character of the Bloch bands. Previously, the measurement of topological invariants was confined to two-dimensional bands by exploiting the relation between the Chern number and the Hall conductivity for a filled band introduced by Thouless-Kohmoto-Nightingale-DeNijs (5). There the integration over the Brillouin zone necessary to determine the topological invariant was achieved through filling of the underlying Bloch band. In con-

trast, in our case the integration over the Brillouin zone necessary for extracting topological invariants is achieved by adiabatic transport of a single-particle wave packet through the band using Bloch oscillations. Recently, it has also been suggested that in the context of ultra-cold atoms, topological properties could be studied through time-of-flight images (17–19) or measurements of anomalous velocity (6, 20).

In the following we focus on a dimerized optical lattice with two sites per unit cell – a system which, despite its simplicity, exhibits rich topological physics, and depending on the parameter values can mimic either polyacetylene (3), or conjugated diatomic polymers (16). Within a tight-binding model, the physics of such a system is captured by the Rice-Mele Hamiltonian (16):

$$\hat{H} = - \sum_n \left( J \hat{a}_n^\dagger \hat{b}_n + J' \hat{a}_n^\dagger \hat{b}_{n-1} + \text{h.c.} \right) + \Delta \sum_n (\hat{a}_n^\dagger \hat{a}_n - \hat{b}_n^\dagger \hat{b}_n), \quad (2)$$

where  $J, J'$  denote modulated tunneling amplitudes within the unit cell,  $\hat{a}_n^\dagger (\hat{b}_n^\dagger)$  are the particle creation operators for an atom on the sublattice site  $a_n (b_n)$  in the  $n$ th lattice cell (Fig. 1a), and  $\Delta$  characterizes the energy offset between neighboring lattice sites.

When the on-site energies of the two sites are tuned to be equal ( $\Delta = 0$ ), our system corresponds to the SSH model of polyacetylene (see Fig. 1a). In this case,  $\hat{H}$  is known to exhibit two topologically distinct phases, D1 for  $J > J'$ , and D2 for  $J < J'$ , separated by a topological phase transition point at  $J = J'$ . The distinct topological character of the two phases is reflected in the difference of their Zak phases, for which  $\delta\varphi_{\text{Zak}} = \pi$ . When the on-site energies are tuned to be different ( $\Delta \neq 0$ ), our system models a linearly conjugated diatomic polymer; in this case, the difference of the Zak phases is fractional in units of  $\pi$ .

In the experiment, we realized the Hamiltonian  $\hat{H}$  of Eq. (2) by loading a Bose-Einstein condensate of  $^{87}\text{Rb}$  into a one-dimensional optical superlattice potential (21). This potential was formed by superim-

posing two standing optical waves of wavelengths  $\lambda_s = 767$  nm and  $\lambda_l = 2\lambda_s = 1534$  nm that generate a lattice potential of the form  $V(x) = V_l \sin^2(k_l x + \phi/2) + V_s \sin^2(2k_l x + \pi/2)$ , where  $k_l = 2\pi/\lambda_l$  (Fig. 1a). Phase control between the two standing wave fields enabled us to fully control  $\phi$ . For example, switching between  $\phi = 0$  and  $\phi = \pi$  allowed us to rapidly access the two different dimerized configurations D1 (D2) with  $\Delta = 0$  in the experiment, whereas by tuning  $\phi$  slightly away from these symmetry points, we could introduce a controlled energy offset  $\Delta$ .

The eigenstates of  $\hat{H}$  can be written as Bloch waves of the form:

$$\psi_k(x) = e^{ikx} u_k(x) = \sum_n \alpha_k e^{ikx_n} w_a(x - x_n) + \beta_k e^{ik(x_n + d/2)} w_b(x - x_n - d/2),$$

where  $k$  denotes the quasimomentum,  $x_n = nd$  with  $n$  integer, and  $w_{a,b}(x)$  are the Wannier functions (22) for  $a_n, b_n$  sites, respectively. The coefficients  $\alpha_k, \beta_k$  are determined through the eigenvalue equation  $\hat{H}\psi_k = E_k\psi_k$ . In this case, the cell-periodic wave function  $u_k$  can be viewed as a two-component spinor  $\mathbf{u}_k = (\alpha_k, \beta_k)$ , and Eq. (1) for the Zak phase takes an especially simple form:

$$\varphi_{\text{Zak}} = i \int_{-G/2}^{G/2} (\alpha_k^* \partial_k \alpha_k + \beta_k^* \partial_k \beta_k) dk.$$

For our choice of the unit cell (Supplementary Information), the eigenfunctions for the lower (upper) band of the SSH model ( $\Delta = 0$ ) are

$$\mathbf{u}_{\mp, k} = \frac{1}{\sqrt{2}} \begin{pmatrix} \pm 1 \\ e^{-i\theta_k} \end{pmatrix},$$

where  $\theta_k$  is determined through  $J e^{ikd/2} + J' e^{-ikd/2} = |\varepsilon_k| e^{i\theta_k}$  (Supplementary Information). We can thus visualize the Bloch periodic functions as pseudo spin-1/2 states oriented in the equatorial plane of a Bloch sphere (Fig. 1c). Note also that although  $\psi_{k+G}(x) = \psi_k(x)$ , this translational invariance is not true for  $\mathbf{u}_{\mp, k}$ , because in our system with a two-site unit cell  $\mathbf{u}_{\mp, k+G} = \hat{\sigma}_z \mathbf{u}_{\mp, k}$ , where  $\hat{\sigma}_z$  is the third Pauli matrix. As the two state vectors for the upper and lower bands are orthogonal, they point

in opposite directions and therefore exhibit the same winding when the quasimomentum  $k$  is varied adiabatically. The Zak phases for the lower and upper band are thus identical  $\varphi_{\text{Zak}}^{D1} = \pi/2$ . However, when the dimerization is changed from configuration D1 to D2 (Fig. 1c), the corresponding geometric phase changes to  $\varphi_{\text{Zak}}^{D2} = -\pi/2$ , because of the opposite winding of the state with quasimomentum  $k$ . The difference of the two Zak phases for the two dimerized configurations is then:

$$\delta\varphi_{\text{Zak}} = \varphi_{\text{Zak}}^{D1} - \varphi_{\text{Zak}}^{D2} = \pi. \quad (3)$$

We point out that the Zak phase of each dimerization is a gauge dependent quantity, i.e. it depends on the choice of origin of the unit cell, however, the difference of Zak phases of the two dimerizations is uniquely defined (8, 23). There is, however, a natural choice of the origin of the unit cell with which one can identify which dimerization configuration is topologically trivial or non-trivial (See Section X in the Supplementary Information).

When an atom is adiabatically evolved through the Brillouin zone of the periodic potential  $k \rightarrow k+G$ , it acquires a phase shift due to three distinct contributions: i) a geometric phase  $\varphi_{\text{Zak}}$  as well as ii) a dynamical phase  $\varphi_{\text{dyn}} = \int E(t)/\hbar dt$ , both derived from the band-structure, and iii) a phase due to the Zeeman energy of the atom in an external magnetic field (see semiclassical analysis in the Supplementary Information):

$$\varphi_{\text{tot}} = \varphi_{\text{Zak}} + \varphi_{\text{dyn}} + \varphi_{\text{Zeeman}}.$$

To isolate the geometrical Zak phase in the experiment, we employ a three-step sequence (Fig. 2a and Supplementary Information). Step 1) We start with an atom in the state  $|\downarrow, k=0\rangle$  and bring it into a coherent superposition state  $1/\sqrt{2}(|\uparrow, k=0\rangle + |\downarrow, k=0\rangle)$  using a microwave  $\pi/2$ -pulse. Here  $\sigma = \uparrow, \downarrow$  denote two spin states of the atom with opposite magnetic moment. Then a magnetic field gradient is applied that creates a constant force in opposite directions for the two spin components. Such a constant force leads to Bloch oscillations, i.e. a linear evolution of quasimomentum over time (24). In our case the force is directed in opposite directions for the two spin components. The atomic wavepacket thus

evolves into the coherent superposition state  $1/\sqrt{2}(|\uparrow, k\rangle + e^{i\delta\varphi}|\downarrow, -k\rangle)$ . When both reach the band edge, the differential phase between the two states is given by  $\delta\varphi = \varphi_{\text{Zak}} + \delta\varphi_{\text{Zeeman}}$ . Note that for all time-reversal invariant Hamiltonians (as it is the case here), the dynamical phase acquired during the adiabatic evolution is equal for the two spin states and therefore cancels in the phase difference. In principle, if a sufficiently high magnetic field stability is present in the laboratory such that  $\varphi_{\text{Zeeman}}$  is reproducible, one could end the experimental sequence here by applying a second  $\pi/2$ -pulse with phase  $\varphi_{MW}$  as described in step 3 below. The Zak phase of the lowest band could then be directly extracted from the resulting Ramsey fringe. Step 2) To eliminate the Zeeman phase difference, we apply a spin-echo  $\pi$ -pulse at this point and also switch dimerization from  $D1 \rightarrow D2$ . For atoms located at the band edge  $k = \pm G/2$ , this non-adiabatic dimerization switch induces a transition to the excited band of the SSH model. Step 3) The sequence is finally completed by letting the spin components further evolve in the upper band until they return to  $k = 0$ . At this point in time, a final  $\pi/2$ -pulse with phase  $\varphi_{MW}$  is applied in order to interfere the two spin components and read out their relative phase  $\delta\varphi$  through the resulting Ramsey fringe. The change in dimerization occurring at the mid-point of the echo sequence is crucial in order not to cancel the Zak phase in addition to the Zeeman phase. Due to the opposite windings of the Bloch states in the upper and lower bands with quasimomentum  $k$  (Fig. 1c), the resulting phase shift encoded in the Ramsey fringe is thus given by:  $\delta\varphi = \varphi_{\text{Zak}}^{D1} - \varphi_{\text{Zak}}^{D2}$  if the dimerization is swapped, whereas  $\delta\varphi = 0$  if it is left unchanged.

In Fig. 2b,c we show images of the momentum distribution of the atoms during the spin-dependent Bloch oscillations in the lower and upper energy bands. Note the opposite evolution in momentum space due to the opposite magnetic moments of the two spin-states. Atoms in the upper energy band are characterized by a distinctively different momentum pattern from atoms in the lower energy band. The Bloch oscillations period of  $\tau_{\text{Bloch}} = 0.85(3)$  ms was chosen to be slow enough, such that non-adiabatic Landau-Zener transitions at the band edge are negligible, while still maintaining an overall fast evolution time to minimize decoherence effects.

A typical result for the two Ramsey fringes obtained with and without dimerization swapping during the state evolution can be seen in Fig. 3a. Each plotted value for a given angle  $\varphi_{MW}$  is an average over five identical measurements in order to reduce the effect of residual fluctuations. We performed a further statistical analysis by recording 14 independent Ramsey fringes for the two configurations. The obtained phase differences are shown in Fig. 3b together with the corresponding histogram. From these individual measurements we determine the geometric phase difference between the two dimerized configurations to be:

$$\delta\varphi = 0.97(2)\pi,$$

in excellent agreement with theory, as discussed above. The uncertainty in the recorded value denotes the standard error of the mean obtained from the distribution function (Fig. 3b) and it is mainly determined by experimental imperfections in the control of the underlying lattice potentials, particularly of the relative phase  $\phi$  between the two standing waves.

To further demonstrate the generality of our method, we studied the dependence of the Zak phase on a staggered on-site energy  $\Delta$  (Fig. 4a and Eq. 2). This corresponds to a heteropolar dimer configuration (16), where the value of the Zak phase is non-quantized. The energy offset  $\Delta$  displaces the pseudo-spin Bloch vectors away from the equatorial plane:

$$\mathbf{u}_{-,k} = \begin{pmatrix} \sin \frac{\gamma_k}{2} \\ \cos \frac{\gamma_k}{2} e^{-i\theta_k} \end{pmatrix}, \quad \mathbf{u}_{+,k} = \begin{pmatrix} -\cos \frac{\gamma_k}{2} \\ \sin \frac{\gamma_k}{2} e^{-i\theta_k} \end{pmatrix}, \quad \gamma_k = \arctan \frac{\varepsilon_k}{\Delta}, \quad (4)$$

resulting in an additional dependence of the Zak phase on the offset  $\Delta$  and the band index (Fig. 4a and Supplementary Information).

In order to probe the dependence of  $\varphi_{\text{Zak}}$  on  $\Delta$ , we performed an experimental sequence that was similar to the one described above. However, instead of swapping the dimerization from D1 to D2, an energy offset  $|\Delta| < 2J$  was introduced for one half of the sequence. Thereafter, because of the spin-echo pulse, the wavepackets return to  $k = 0$  in the lowest band. Though the system completes a full Bloch oscillation in

the lowest band, the total geometric phase acquired is not zero, since the Bloch vector is displaced from the equatorial plane during one half of the sequence (Fig. 4) and the Zak phase is changed from  $\varphi_{\text{Zak}}$  to  $\varphi_{\text{Zak}}(\Delta)$ . The resulting phase in the Ramsey fringe is thus given by  $\delta\varphi = \varphi_{\text{Zak}} - \varphi_{\text{Zak}}(\Delta)$  when the energy offset is present, and it is  $\delta\varphi = 0$  when the offset is absent. As before, the phase difference between these two fringes for atoms in the lowest band allows us to determine the relative phase  $\varphi_{\text{Zak}} - \varphi_{\text{Zak}}(\Delta)$ . During the non-adiabatic switching of the superlattice potential at step 2 of the experimental sequence some of the atoms are transferred to the higher band and acquire a different geometric phase. However, taking into account this contribution to the measured phase difference enabled us to extract the relative phase  $\delta\varphi$  from our data (see Supplementary Information). As shown in Fig. 4b, we find good agreement between the measured and predicted values of the fractional Zak phase. Fractional Zak phases could also be determined by carrying out one full Bloch oscillation cycle for each of the spin states. The dynamical phase would then be cancelled even for general lattice structures without time-reversal symmetry and the resulting Ramsey phase corresponds to  $2\varphi_{\text{Zak}}$ .

In conclusion, we have presented a general approach for studying topological properties of Bloch bands in optical lattices and demonstrated its versatility through a first measurement of the topological invariant in topologically non-trivial Bloch bands. Topologically distinct many-body phases can arise from such topologically distinct Bloch bands when the bands are filled with fermions. Making use of the recently demonstrated control of optical potentials at the single-site level (25), we plan to realize domain walls or sharp boundaries in the dimerized lattice that would allow us to directly study edge states (26,27) and fractional charges for non-interacting fermions or hardcore bosons (1–3, 28, 29). Although in this work we focused on one-dimensional systems, our technique can easily be extended to two-dimensional systems, where the change of the Zak phase in the Brillouin zone gives the topological density of the Bloch band (30). This enables measurements of both the Chern number of topological bands and the  $\pi$ -flux associated with a Dirac point. Additionally, we expect that this idea can be extended to measure the

non-Abelian Berry's phase in Bloch bands, such as in a system with quantum spin Hall effect (31), to the study of Floquet states in periodically driven systems (32–34), and to quasiparticles in unconventional superconductors, such as *d*-wave superconductors, which have Dirac dispersion at the nodal points (35). Overall, our work indicates that cold atomic systems provide a versatile platform for studying topological states of matter, and establishes a novel method for probing their properties.

We acknowledge helpful discussions with B. Paredes. We thank Yu-Ao Chen and Sylvain Nascimbène for their help in setting up the experiment and for their comments in early stages of the experiment. This work was supported by the DFG (FOR635, FOR801), NIM and DARPA (OLE program). M. Aidelsburger was additionally supported by the Deutsche Telekom Stiftung.

## References and Notes

1. R. Jackiw and C. Rebbi. Solitons with fermion number  $1/2$ . Phys. Rev. D 13, 3398 (1976).
2. J. Goldstone and F. Wilczek. Fractional Quantum Numbers on Solitons. Phys. Rev. Lett. 47, 986-989 (1981).
3. W. P. Su, J. R. Schrieffer, and A. J. Heeger. Solitons in Polyacetylene. Phys. Rev. Lett. 42, 1698-1701 (1979).
4. J. S. Bell and R. Rajaraman. On states, on a lattice, with half-integer charge. Nucl. Phys. B, Volume 220, Issue 1, 1-12 (1983).
5. D. J. Thouless, M. Kohmoto, M. P. Nightingale, and M. den Nijs. Quantized Hall Conductance in a Two-Dimensional Periodic Potential. Phys. Rev. Lett. 49, 405-408 (1982).
6. D. Xiao, M.-C. Chang, and Q. Niu. Berry phase effects on electronic properties. Rev. Mod. Phys. 82, 1959-2007 (2010).

7. M. Z. Hasan and C. L. Kane. Colloquium: Topological insulators. *Rev. Mod. Phys.* 82, 3045-3067 (2010).
8. X. Qi and S. Zhang. Topological insulators and superconductors. *Rev. Mod. Phys.* 83, 1057-1110 (2011).
9. M. V. Berry. Quantal phase factors accompanying adiabatic changes. *Proc. Roy. Soc. London A* 392, 45-57 (1984).
10. A. Kitaev. Periodic table for topological insulators and superconductors. *AIP Conference Proceedings* 1134, 22-30 (2009).
11. S. Ryu, A. Schneider, A. Furusaki, and A. Ludwig. Topological insulators and superconductors: tenfold way and dimensional hierarchy. *New J. Phys.* 12, 065010 (2010).
12. J. Zak. Berry's phase for energy bands in solids. *Phys. Rev. Lett.* 62, 2747-2750 (1989).
13. S. Ryu, Y. Hatsugai. Topological Origin of Zero-Energy Edge States in Particle-Hole Symmetric Systems. *Phys. Rev. Lett.* 89, 077002 (2002).
14. P. Delplace, D. Ullmo, and G. Montambaux. Zak phase and the existence of edge states in graphene. *Phys. Rev. B* 84, 195452 (2011).
15. A. J. Niemi and G. W. Semenoff. Spectral asymmetry on an open space. *Phys. Rev. D* 30, 809-818 (1984).
16. M. J. Rice and E. J. Mele. Elementary Excitations of a Linearly Conjugated Diatomic Polymer. *Phys. Rev. Lett.* 49, 1455-1459 (1982).
17. E. Alba *et al.* Seeing Topological Order in Time-of-Flight Measurements. *Phys. Rev. Lett.* 107, 235301 (2011).

18. E. Zhao *et al.* Chern numbers hiding in time-of-flight images. *Phys. Rev. A* 84, 063629 (2011).
19. N. Goldman *et al.* Measuring topology in a laser-coupled honeycomb lattice: from Chern insulators to topological semi-metals. *New J. Phys.* 15, 013025 (2013).
20. H.M. Price and N.R. Cooper. Mapping the Berry curvature from semiclassical dynamics in optical lattices. *Phys. Rev. A* 85, 033620 (2012).
21. S. Fölling *et al.* Direct observation of second-order atom tunnelling. *Nature* 448, 1029-1032 (2007).
22. G. H. Wannier. Dynamics of Band Electrons in Electric and Magnetic Fields. *Rev. Mod. Phys.* 34, 645-655 (1962).
23. R. D. King-Smith and D. Vanderbilt. Theory of polarization of crystalline solids. *Phys. Rev. B* 47, 1651-1654 (1993).
24. M. Ben Dahan, E. Peik, J. Reichel, Y. Castin, and Ch. Salomon. Bloch Oscillations of Atoms in an Optical Potential. *Phys. Rev. Lett.* 76, 4508-4511 (1996).
25. C. Weitenberg *et al.* Single-spin addressing in an atomic Mott insulator. *Nature* 471, 319-324 (2011).
26. T. Kitagawa *et al.* Observation of topologically protected bound states in photonic quantum walks. *Nature Comm.* 3, 882 (2012).
27. Y.E. Kraus *et al.* Topological States and Adiabatic Pumping in Quasicrystals. *Phys. Rev. Lett.* 109, 106402 (2012).
28. J. Ruostekoski, G. Dunne, and J. Javanainen. Particle Number Fractionalization of an Atomic Fermi-Dirac Gas in an Optical Lattice. *Phys. Rev. Lett.* 88, 180401 (2002).
29. F. Grusdt, M. Hoening, and M. Fleischhauer. Topological edge states in the one-dimensional superlattice Bose-Hubbard model. [arXiv:1301.7242](https://arxiv.org/abs/1301.7242)

30. D. Abanin *et al.* Interferometric Approach to Measuring Band Topology in 2D Optical Lattices. Phys. Rev. Lett. 110, 165304 (2013)
31. C.L. Kane and E.J. Mele. Quantum Spin Hall Effect in Graphene. Phys. Rev. Lett. 95, 226801 (2005).
32. M. Grifoni and P. Hänggi. Driven quantum tunneling. Phys. Rep. 304, Issue 5-6, 229-354 (1998).
33. T. Kitagawa, E. Berg, M. Rudner, and E. Demler. Topological characterization of periodically driven quantum systems. Phys. Rev. B 82, 235114 (2010).
34. N.H. Lindner, G. Refael and V. Galitski. Floquet topological insulator in semiconductor quantum wells. Nature Phys. 7, 490-495 (2011).
35. G.E. Volovik, *The Universe in a Helium Droplet*, Oxford University Press (2003).

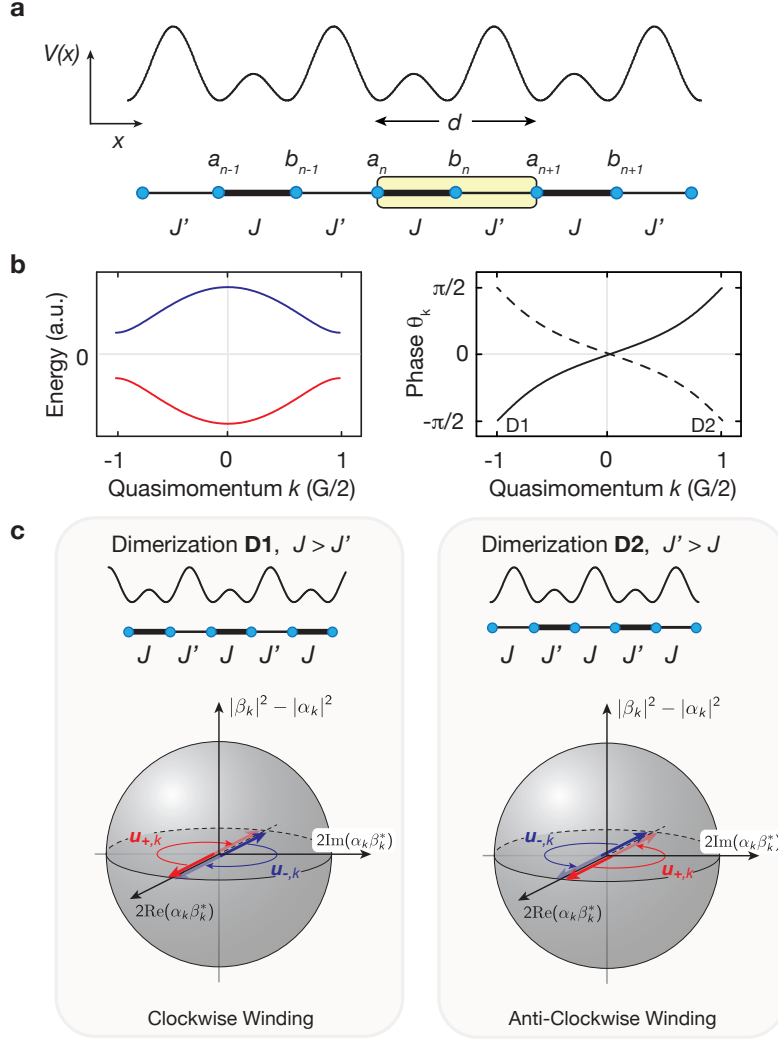


**Figure 1: Energy bands and topology of dimerized lattice model.** **a**, Schematic illustration of optical superlattice potential used in the experiment to realize the Su-Schrieffer-Heeger model (yellow box denotes the unit cell of size  $d = \lambda_s$ ). **b**, Exemplary curves for the lower and upper energy bands (red and blue lines) and phase  $\theta_k$  for dimerization D1 and D2 (solid and dashed line) as a function of quasimomentum  $k$ . **c**, Pseudo-spin representation of the eigenstates  $\mathbf{u}_{\mp, k}$  of the upper and lower energy bands for the two dimerization configurations D1 and D2. The pseudo-spin vectors  $\mathbf{u}_{\mp, k}$  point in opposite directions and exhibit the same sense of rotation (winding) with quasimomentum  $k$ . In the phase D1 (D2)  $\mathbf{u}_{\mp, k}$  evolve (anti-) clockwise and therefore exhibit opposite winding.

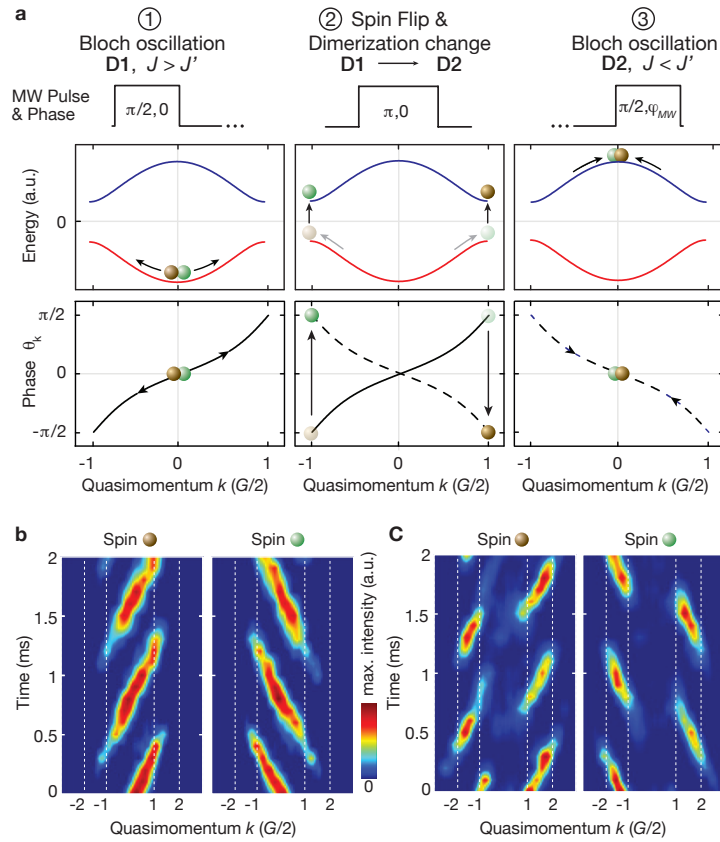


**Figure 2: Experimental sequence and spin-dependent Bloch oscillations.** **a**, Energy band, MW pulses and state evolution of a single atom in a superposition of two spin-states with opposite magnetic moment (brown and green balls) during the three-step echo sequence described in the text. The winding of the state vector with  $k$  is given by  $\theta_k$  (solid line dimerization D1, dashed line dimerization D2). **b,c**, Time-of-flight momentum distributions taken for different evolution times of the spin-dependent Bloch oscillations in the lower (b) and upper energy band (c) used in the experiment. Each momentum point is an average of three identical measurements.

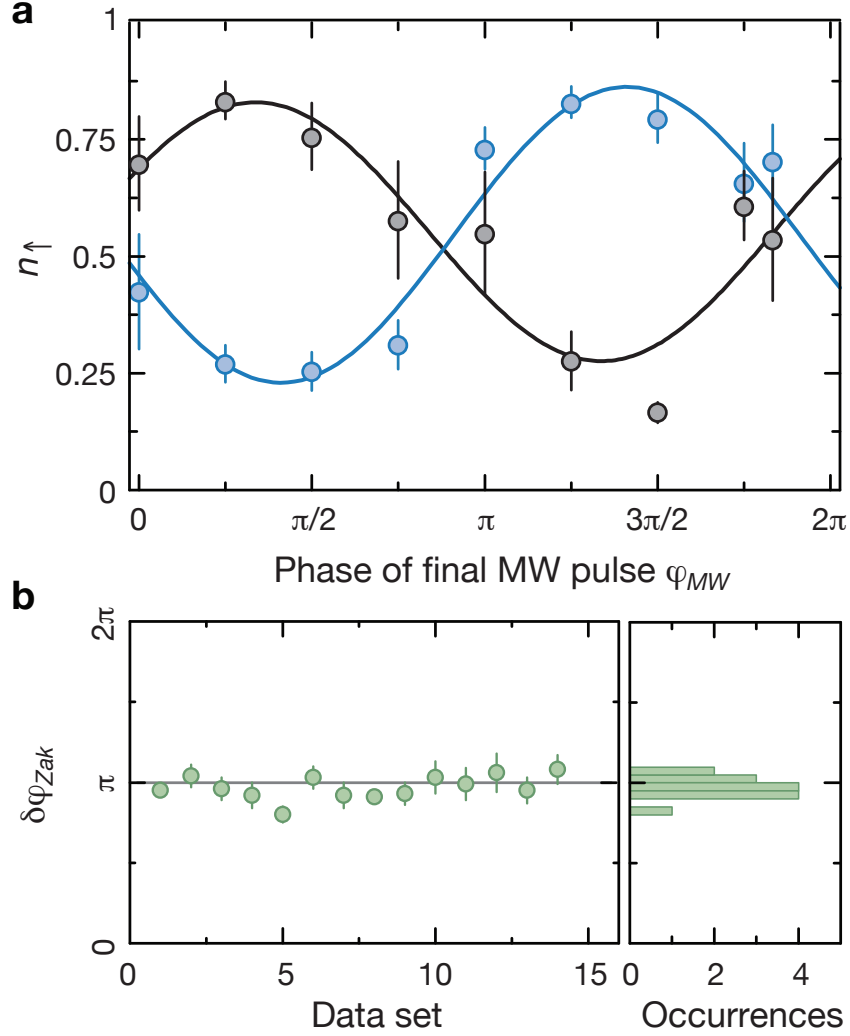


**Figure 3: Determination of the Zak phase.** **a**, Following the sequence described in the text, the atom number in the two spin states  $N_{\uparrow,\downarrow}$  is measured and the fraction of atoms in the  $|\uparrow\rangle$  spin state  $n_\uparrow = N_\uparrow/(N_\uparrow + N_\downarrow)$  is plotted as a function of the phase of the final microwave  $\pi/2$ -pulse. Blue (black) circles correspond to the fringe in which the dimerization was (not) swapped, and the corresponding solid lines are sinusoidal fits to the data, where the free parameters were the amplitude, offset and initial phase. The difference in phase of the two fits to the Ramsey fringes yields the Zak phase difference  $\delta\varphi_{Zak} = \varphi_{Zak}^{D1} - \varphi_{Zak}^{D2}$ . In order to reduce the effect of fluctuations, every data point is an average of five individual measurements and the error bars show the standard deviation of the mean. The phase of the reference fringe (black) is determined by a small detuning of the microwave pulse (Supplementary Information). **b**, Measured relative phase for 14 identical experimental runs (left), which give an average value of  $\delta\varphi_{Zak} = 0.97(2)\pi$ . The corresponding histogram is shown on the right with a binning of  $0.05\pi$ . The  $1\sigma$ -width of the resulting distribution is  $\sigma = 0.07\pi$ .

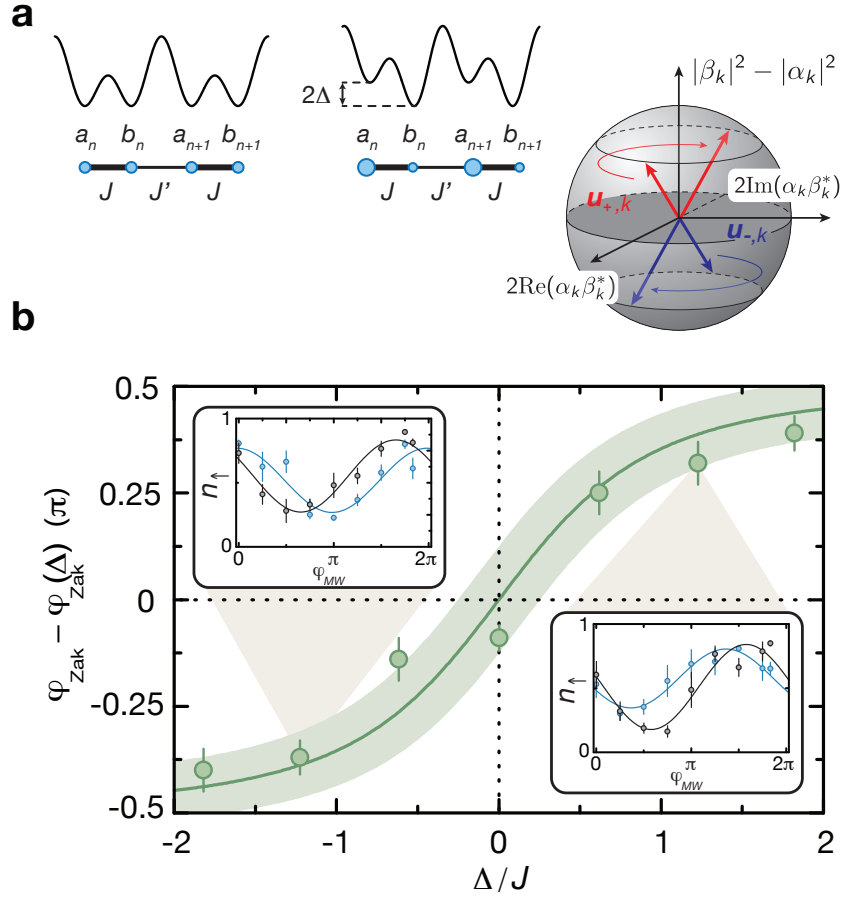


Figure 4: **Fractional Zak phase.** **a**, Lattice potential without and with an on-site energy staggering  $\Delta$ . When  $\Delta = 0$  the Zak phase is  $\varphi_{\text{Zak}}(\Delta = 0) = \pi/2$ . As  $\Delta$  increases, the pseudo-spin vectors move away from the equatorial plane and the value of  $\varphi_{\text{Zak}}(\Delta)$  decays rapidly to zero. **b**, Measured phase difference  $\varphi_{\text{Zak}} - \varphi_{\text{Zak}}(\Delta)$  as a function of  $\Delta$ . Each individual point was obtained from four individual measurements. The vertical error bars represent the standard error of the mean. The green line is the theoretical prediction and the shaded area represents the uncertainties in the calibration of the energy offset  $\Delta$ . The insets show a typical Ramsey fringe for  $\Delta/J = -1.2$  (left) and  $\Delta/J = 1.2$  (right), which were used to extract the relative phase  $\delta\varphi$ . The blue (black) fringes correspond to measurements with (without) staggering (Supplementary Information).